



Universiteit
Leiden
The Netherlands

The synthesis and biological applications of photo-activated ruthenium anticancer drugs

Lameijer, L.N.

Citation

Lameijer, L. N. (2017, December 14). *The synthesis and biological applications of photo-activated ruthenium anticancer drugs*. Retrieved from <https://hdl.handle.net/1887/58398>

Version: Not Applicable (or Unknown)

License: [Licence agreement concerning inclusion of doctoral thesis in the Institutional Repository of the University of Leiden](#)

Downloaded from: <https://hdl.handle.net/1887/58398>

Note: To cite this publication please use the final published version (if applicable).

Cover Page



Universiteit Leiden



The handle <http://hdl.handle.net/1887/58398> holds various files of this Leiden University dissertation.

Author: Lameijer, L.N.

Title: The synthesis and biological applications of photo-activated ruthenium anticancer drugs

Issue Date: 2017-12-14

Chapter 3:

D- versus L-glucose conjugation

Mitochondrial targeting of a light-activated, dual-mode of action ruthenium-based anticancer prodrug

Abstract: Light-activated ruthenium polypyridyl anticancer prodrugs often suffer from poor water solubility, poor selectivity, and/or ill-defined intracellular targets. Coordination of the D- or L-glucose thioether ligand **3** = 2-(2-(2-(methylthio)ethoxy)ethoxy)ethyl- β -glucopyranoside to the highly lipophilic ruthenium complex $[\text{Ru}(\text{tpy})(\text{dppn})(\text{OH}_2)]^{2+}$ (**[1]**²⁺, tpy = 2,2':6',2''-terpyridine, dppn = benzo[*l*]dipyrido-[3,2-*a*:2',3'-*c*]phenazine) solved all problems at once. The two enantiomers $[\text{Ru}(\text{tpy})(\text{dppn})(\textbf{3})](\text{PF}_6)_2$ (**[D-2]**(PF₆)₂ and **[L-2]**(PF₆)₂) are soluble in water, which allowed for probing the influence of the chirality of the glucose moiety on uptake, toxicity, and intracellular localization of the prodrug without changing any other physical and/or chemical properties. Both compounds showed mild but different cytotoxicity in A549 (human lung carcinoma) and MCF-7 (human breast adenocarcinoma) cancer cells in the dark, whereas similarly high cytotoxicity was observed for both compounds after irradiation with low doses of visible light (3.1 J.cm⁻² at 455 nm). Irrespective of chirality the slightly emissive Ru complexes were found in the mitochondria, where two modes of action may contribute to light-induced cell death. On the one hand, the glucose-thioether ligand is photosubstituted by water, thus releasing **[1]**²⁺ that interacts with DNA at an exceptionally high 400:1 bp:Ru ratio. On the other hand, both **[2]**²⁺ and **[1]**²⁺ produce large amounts of singlet oxygen, leading to very efficient photocleavage of DNA.

This work was published as a full paper: L. N. Lameijer, S. L. Hopkins, T. G. Brevé, S. H. C. Askes, S. Bonnet, *Chem. Eur. J.* **2016**, 22, 18484-18491.

3.1 Introduction

One of the major challenges in the development of new anticancer drugs is to improve selectivity. A common strategy to better differentiate normal proliferating cells from malignant cells is to develop drugs targeting specific hallmarks of cancer cells, such as aerobic glycolysis. As first described by Otto Warburg,^[1] cancer cells use glycolysis for their energy production and therefore have a higher demand for simple sugars such as D-glucose. As the cell membrane is impermeable to polar molecules specific membrane transporters control glucose uptake (GLUT and SGLT). These transporters are overexpressed in many cancer cell types, which not only aids D-glucose penetrating into the cell, but also provides a method to target imaging or therapeutic compounds to cancer cells.^[2] For example, 2-deoxy-2-(¹⁸F)fluoro-D-glucose (18-FDG) is a common radiotracer used in the clinics to image tumors *in vivo*.^[3] Conjugating D-glucose or other GLUT substrates to organic^[3-4] or inorganic^[5] anticancer compounds is a quickly expanding cancer-targeting strategy. Several methods have been proposed to assess the benefits of D-glucose functionalization of an anticancer drug. Enhanced uptake is usually demonstrated indirectly, for example by comparing glucose-functionalized drugs to their aglycon counterpart,^[6] or by competitive inhibition experiments with D-glucose.^[7] However, these methods usually ignore the difference in polarity and hydrophilicity between the glycoconjugates and aglycon analogues, which for many compounds can have major influence on drug uptake, localization, and/or mode-of-action. Comparing the biological effects of a glycoconjugate on different cell lines with different expressions of glucose transporters is another alternative.^[8] However, depending on the cell line different glucose transporters may be overexpressed,^[9] which complicates the interpretation of such experiments. Finally, adding glucose transporter inhibitors to switch off the uptake of glucose functionalized compounds, is also possible.^[10] However, synergies between biologically active compounds have been demonstrated on multiple occasions,^[11] and it may be difficult to distinguish impaired drug uptake due to the inhibitors, from the cytotoxicity of the inhibitor itself.^[12]

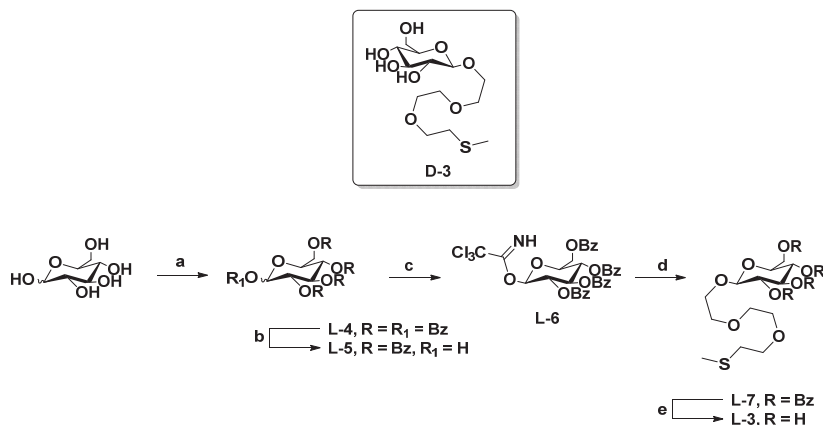
To solve these biases we herein propose a new approach consisting in directly comparing the activity of the D- and L-glucose conjugates of the same drug, here an achiral, highly lipophilic ruthenium compound [Ru(tpy)(dppn)(OH₂)]²⁺ (**1**)²⁺, Scheme 3.2, tpy = 2,2':6',2''-terpyridine, dppn = benzo[*i*]dipyrido-[3,2-*a*:2',3'-*c*]phenazine). Contrary to D-glucose, L-glucose is not a substrate for the glucose transport system.^[13] Our basic assumption was that a L-glucose-modified drug will have the same structural properties and therefore the same polarity and hydrophilicity as its D-glucose analogue but will not be recognized by cellular enzymes due to its different chirality. Therefore it might be possible to probe the biological effects of the D-glucose functional group without the experimental biases mentioned above. Compound **1**)²⁺ has another interesting property: it belongs to a family of metallodrugs that can be activated by visible light irradiation.^[14] Light-activatable

anticancer compounds have been proposed as a way to improve the selectivity of anticancer treatments by an external trigger that limit the toxicity of the treatment to the time and place of light irradiation.^[15] We thus designed the two light-activatable prodrugs $[\text{Ru}(\text{tpy})(\text{dppn})(\text{D-3})]^{2+}$ and $[\text{Ru}(\text{tpy})(\text{dppn})(\text{L-3})]^{2+}$ ($[\text{D-2}]^{2+}$ or $[\text{L-2}]^{2+}$, respectively), where **3** is a thioether ligand covalently linked to D- or L-glucose that binds to ruthenium *via* a thermally stable Ru-S coordination bond (Scheme 3.2). The synthesis, photochemistry, and biological evaluation of these enantiomeric ruthenium compounds is reported, and their cytotoxicity, cellular distribution, and mode-of-action, are discussed.

3.2 Results and Discussion

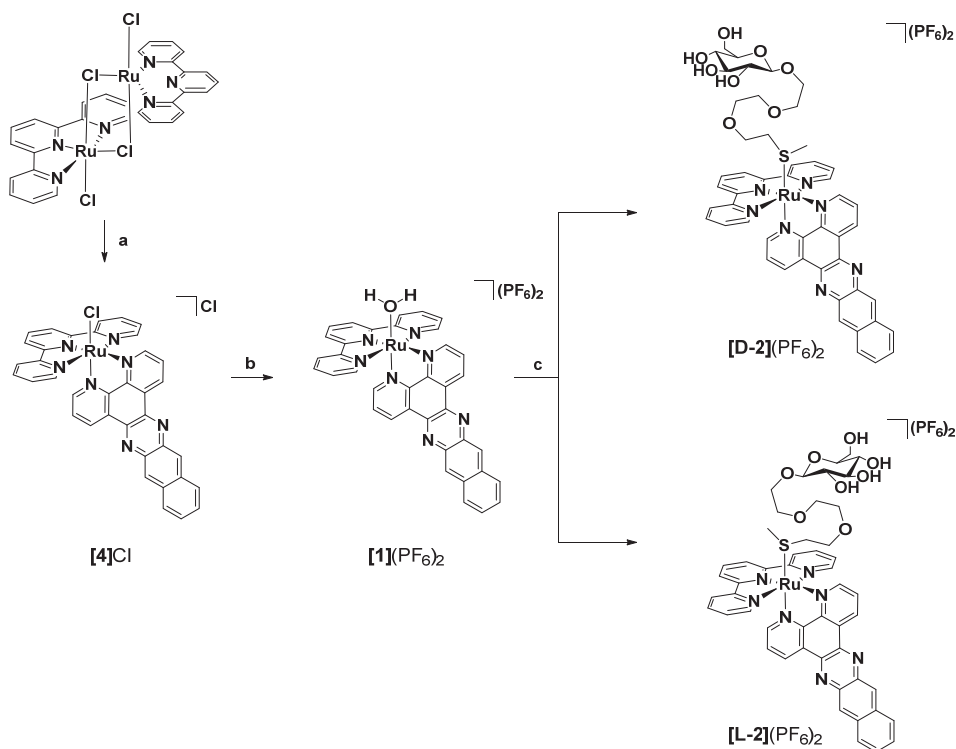
3.2.1 Synthesis

The thioether-glucose conjugates **D-3** (Chapter 2) and **L-3** (Scheme 3.1) were synthesized from D- and L-glucose, respectively, according to the Schmidt methodology.^[16] As expected both ligands were found to have the same physical and spectroscopic properties, except for their opposite sign of optical rotation (**D-3**: $[\alpha]_D^{20}$ -10.0 ($c = 1.00$ in MeOH) and **L-3**: $[\alpha]_D^{20}$ +11.8 ($c = 1.00$ in MeOH) and their different retention time on chiral HPLC (Figure S.II.13 and S.II.14).



Scheme 3.1 a). BzCl in pyridine, 0 °C – rt, 6 h, quant.; b). i. 33% HBr/AcOH in DCM, rt, overnight; ii. Ag_2CO_3 in acetone/water, rt, 3 h, 99% over two steps; c). trichloroacetonitrile, DBU in DCM, rt, overnight, 78%; d). 2-(2-(2-(methylthio)ethoxy)ethoxy)ethan-1-ol, DCM, cat. TMSOTf, rt, 3 h, 69%; e). cat. NaOMe in MeOH, rt, overnight, 85%.

In a second step, the ligands **D-3** or **L-3** were coordinated to ruthenium according to Scheme 3.2. Isolation of the aqua complex, $[\mathbf{1}](\text{PF}_6)_2$ was necessary, and further reaction with a three-fold excess of **D-3** or **L-3** under mild conditions (acetone, 50 °C) afforded the D- and L-glucose conjugates $[\text{D-2}](\text{PF}_6)_2$ and $[\text{L-2}](\text{PF}_6)_2$ in moderate yields (32% and 35% respectively). Unlike $[\mathbf{1}](\text{PF}_6)_2$ and $[\text{Ru}(\text{tpy})(\text{dppn})\text{Cl}]\text{Cl}$ (**[4]Cl**), which are virtually insoluble in water, $[\text{D-2}](\text{PF}_6)_2$ and $[\text{L-2}](\text{PF}_6)_2$ can be dissolved in water even in absence of DMSO.



Scheme 3.2 Synthesis of $[D-2](PF_6)_2$ and $[L-2](PF_6)_2$. a). 2 eq. dppn in ethylene glycol, 5 hr, 100 °C, 75%; b). i. 1.0 eq. $AgNO_3$ in acetone/water (3:1), 50 °C; ii. NH_4PF_6 , 84%; c). 2.66 eq. **D-3** or **L-3** in acetone, 50 °C, 24 h, 35% for $[D-2](PF_6)_2$ and 32% for $[L-2](PF_6)_2$.

3.2.2 Photochemistry

The photoreactivity of the water-soluble thioether complex $[D-2](PF_6)_2$ was tested in different conditions. Figure 3.1 shows the evolution of the UV-vis spectrum of $[D-2](PF_6)_2$ upon blue light irradiation (450 nm) in pure water and under argon. The initial absorption maximum at 460 nm decreased while a new 1MLCT band at 474 nm increased; a clear isosbestic point was also observed, showing that in such conditions a single photoproduct was obtained. According to mass spectrometry, the photoproduct was $[Ru(tpy)(dppn)(OH_2)]^{2+}$ (**[1]²⁺**, m/z = found 342.4, calculated 342.5). Photosubstitution of the thioether-glucose conjugate by water proceeds with a quantum yield of 0.00095 (\pm 0.00002) in deoxygenated water. Usually, such photosubstitution processes significantly reduce the emission of ruthenium polypyridyl complexes. Indeed, the phosphorescence of $[D-2](PF_6)_2$ in PBS (pH = 7.4) and in air under 450 nm excitation was found to be very weak; the wavelength of the emission maximum was 648 nm, and a phosphorescence quantum yield Φ_p of 3.7×10^{-5} was measured. Under prolonged blue light irradiation in air, the wavelength of the emission band shifted from 648 nm to 690 nm, indicating the formation of the also weakly emissive photoproduct **[1]²⁺** ($\Phi_p = 3.2 \times 10^{-5}$). Near-infrared emission

spectroscopy was also performed under 450 nm excitation to check whether irradiating $[\text{D-2}]^{2+}$ in air would produce singlet oxygen. In water, PBS, or D_2O , no emission at 1270 nm was detected because of the very short lifetime of $^1\text{O}_2$ in aqueous solutions. However, in CD_3OD an intense emission peak at 1270 nm, characteristic of singlet oxygen, was observed upon blue light irradiation of $[\text{D-2}](\text{PF}_6)_2$ (Figure S.II.2). The quantum yield of singlet oxygen production (Φ_Δ) of $[\text{D-2}](\text{PF}_6)_2$ in methanol- d_4 was 0.71, *i.e.*, $[\text{D-2}](\text{PF}_6)_2$ generates $^1\text{O}_2$ very efficiently in air (Figure S.II.2). The photoproduct $[\text{Ru}(\text{tpy})(\text{dppn})(\text{CD}_3\text{OD})]^{2+}$, which was obtained after extensive blue light irradiation of $[\text{D-2}]^{2+}$ in CD_3OD , also generated singlet oxygen with a high quantum yield Φ_Δ of 0.43 (Table 3.1).

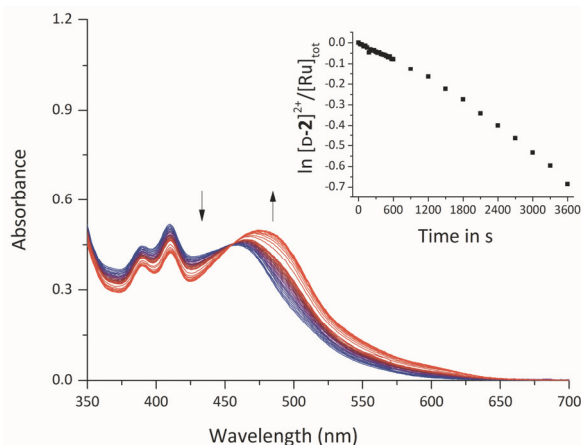


Figure 3.1 Electronic absorption spectra of $[\text{D-2}](\text{PF}_6)_2$ in deoxygenated H_2O irradiated at 450 nm for 60 min. Spectra were taken each 30 s for the first 10 min, followed by a spectrum every 5 min until 60 min. $T = 298\text{ K}$, $[\text{Ru}]_{\text{tot}} = 4.23 \times 10^{-5}\text{ M}$, $\lambda_{\text{exc}} = 450\text{ nm}$, photon flux = $1.77 \times 10^{-7}\text{ mol photons s}^{-1}$. Inset depicts the evolution of $\ln [\text{D-2}]/[\text{Ru}]_{\text{tot}}$ vs. irradiation time.

The results of photosubstitution of the thioether ligand **3** in $[\text{D-2}]^{2+}$ contrast with recent work from the Turro group, who demonstrated that the analogous complex $[\text{Ru}(\text{tpy})(\text{dppn})(\text{pyridine})]^{2+}$ did not undergo photosubstitution of the pyridine ligand in organic solvents. Instead, the complex was reported to efficiently produce $^1\text{O}_2$ ($\Phi_\Delta = 0.98$) due to the presence of low-lying $\pi\text{-}\pi^*$ excited states centered on the dppn ligand.^[17] Apparently, the nature of the monodentate ligand plays an important role in the photoreactivity of this family of dppn-based ruthenium complexes. Although photosubstitution, phosphorescence, and singlet oxygen generation often represent competing pathways in ruthenium photochemistry, when $[\text{D-2}]^{2+}$ is irradiated with blue light all processes may occur, depending on dioxygen concentration. In deoxygenated conditions photosubstitution of the thioether ligand to form the aqua complex is preferred, whereas in air efficient generation of $^1\text{O}_2$ becomes a competing pathway and is observed both before and after photosubstitution.

Table 3.1 Lowest energy absorption maxima, quantum yield for photosubstitution (Φ_{450}), $^1\text{O}_2$ production (Φ_Δ) and phosphorescence (Φ_p) at 298 K.

Complex	$\lambda_{\text{abs}}^{[a]}/\text{nm}$ ($\epsilon/\text{M}^{-1}\text{cm}^{-1}$)	$\Phi_{450}^{[a]}$	$\Phi_\Delta^{[b]}$	$\Phi_p^{[c]}$
[D-2]²⁺	458 (11619)	0.00095 ± 0.00002	0.71	0.000037
[1]²⁺	475 (12643)	-	0.43	0.000032

3.2.3 Cytotoxicity assay

The cytotoxic properties of **[D-2](PF₆)₂** and of its enantiomer **[L-2](PF₆)₂** were tested in the dark on two human cancer cell lines, A549 and MCF-7.^[9] In parallel, considering the dual photoreactivity of **[D-2](PF₆)₂** the phototoxicity of **[D-2](PF₆)₂** and **[L-2](PF₆)₂** was also tested under a low dose of blue light (5 minutes at 454 ± 11 nm, 10.5 ± 0.7 mW · cm⁻², 3.2 ± 0.2 J.cm⁻²). Cells were seeded at $t = 0$ (5×10^3 per well for A549 and 8×10^3 per well for MCF-7), treated with a concentration series of either **[D-2](PF₆)₂** or **[L-2](PF₆)₂** 24 h after seeding, irradiated or maintained in the dark after media refreshment 48 h after seeding, and cell viability was assayed using sulforhodamine B (SRB) 96 h after seeding. The dose-response curves and effective concentrations (EC₅₀) are reported in Figure 3.2 and Table 3.2, respectively. Images of A549 and MCF-7 treated cells (20 μM , **[D-2](PF₆)₂**) 96 h after seeding for dark and irradiated samples are shown in Figures S.II.11 and S.II.12. In the dark the cytotoxicity of **[D-2](PF₆)₂** and **[L-2](PF₆)₂** was significantly different, both for A549 and MCF-7 cells. For **[D-2](PF₆)₂** the effective concentration was 2.6 and 1.9 fold lower for A549 and MCF-7 cells, respectively, than for **[L-2](PF₆)₂** (Table 3.2). Upon light irradiation, both compounds were activated and showed similar high cytotoxicity, characterized by sub-micromolar effective concentrations (EC₅₀). According to these results, the chiral nature of the glucose functional group seems to have an effect on the dark cytotoxicity of the prodrug. In addition, upon light irradiation either the release of the photoproduct **[1]²⁺**, or efficient singlet oxygen generation by the prodrug **[D/L-2]²⁺** and the activated drug **[1]²⁺**, or both, result in a highly cytotoxic combination.^[18]

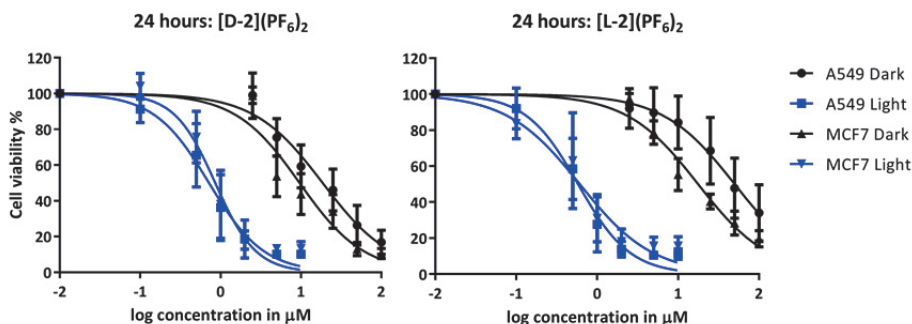


Figure 3.2. Cell viability of A549 and MCF-7 cells versus the logarithm of the concentration of **[D-2](PF₆)₂** and **[L-2](PF₆)₂** in the dark and the light. Data points are means of three independent experiments with \pm SD as error bars.

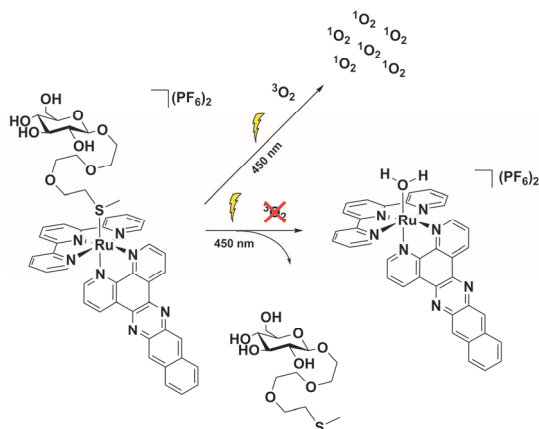


Figure 3.3 Schematic representation of the light-induced dual mode of action for the glycoconjugated compound $[\text{Ru}(\text{tpy})(\text{dppn})(\text{D-3})]^{2+}$ ($[\text{D-2}]^{2+}$), where D-3 is a thioether-glucose conjugate. For clarity the L enantiomers are left out.

Table 3.2 (Photo)cytotoxicity of $[\text{D-2}](\text{PF}_6)_2$ and $[\text{L-2}](\text{PF}_6)_2$ expressed as effective concentrations (EC_{50} in μM) in the dark and after blue light irradiation, and photocytotoxicity index ($\text{PI}^{[\text{c}]}$) versus A549 and MCF-7 cells before and after irradiation with blue light. Values are reported in μM with $\pm 95\%$ Confidence Intervals (CI).

Complex	A549					MCF-7				
	EC_{50} dark ^[a]	$\pm\text{CI}$	EC_{50} 455 nm ^[b]	$\pm\text{CI}$	PI	EC_{50} dark ^[a]	$\pm\text{CI}$	EC_{50} 455 nm ^[b]	$\pm\text{CI}$	PI
$[\text{D-2}](\text{PF}_6)_2$	19	+4.0 -3.3	0.72	+0.16 -0.13	26	9.6	+2.9 -2.3	0.86	+0.21 -0.17	11
$[\text{L-2}](\text{PF}_6)_2$	50	+17 -13	0.58	+0.13 -0.11	86	18	+3.8 -3.1	0.61	+0.28 -0.19	30

[a] Cells were incubated with complexes for 24 h. [b] Cells were incubated with the complex for 24 h, and the media was refreshed before blue light irradiation (5 min at 455 nm with $3.2 \pm 0.2 \text{ J}\cdot\text{cm}^{-2}$). [c] $\text{EC}_{50}(\text{dark})/\text{EC}_{50}(455 \text{ nm})$.

3.2.4 Cellular localization and in vitro imaging

Contrary to many ruthenium complexes capable of photo-substituting one of their ligands, $[\text{D-2}](\text{PF}_6)_2$ and $[\text{L-2}](\text{PF}_6)_2$ were found to be slightly emissive in cells, which allowed for performing uptake and localization studies (Figures 3.4 and S.II.5-S.II.10). Microscopy imaging was performed for A549 cells treated in the dark with $[\text{D-2}](\text{PF}_6)_2$ or $[\text{L-2}](\text{PF}_6)_2$ for 4, 6, and 24 h ($\lambda_{\text{exc}} = 488 \text{ nm}$, Figure S9). These images revealed that independent on incubation time, $[\text{D-2}](\text{PF}_6)_2$ and $[\text{L-2}](\text{PF}_6)_2$ displayed no significant difference in localization or emission intensity, and both complexes were clearly localized outside the nucleus (Figures S.II.5-S.II.6). Co-localization experiments using MitoTracker Deep Red (MTDR, $\lambda_{\text{exc}} = 639 \text{ nm}$) were attempted after 6 h incubation (Figure S.II.9). Due to the weaker emission of $[\text{1}]^{2+}$ compared to MTDR, and some absorption of MTDR at 488 nm, it was impossible to quantitatively co-localize the ruthenium compound and the dye unequivocally. However, the ruthenium compounds and MTDR, added separately, gave qualitatively very similar images using the 488 or 639 nm channels, respectively (Figure 3.4). This suggested that the ruthenium compound might localize in the mitochondria. To confirm that, an experiment was designed where cells were treated with $[\text{D-2}](\text{PF}_6)_2$ at 25

μM in the presence of MTDR. MTDR images were taken at 639 nm, showing normal mitochondrial morphology (Figure S.II.9B and S.II.9E). Then, new images were taken using the 488 nm channel (Figure S.II.9C and S.II.9F), followed by a second set of MTDR images (Figure S.II.9D and S.II.9G). The mitochondria of cells that had been irradiated at 488 nm were altered, showing bubble-like structures, compared to untreated cells. Thus, the combination of treatment with the complexes and 488 nm light irradiation led to modifications of the mitochondria structure. Mitochondria are known to have a highly negative inner membrane potential, which can be targeted by cationic, lipophilic compounds.^[18] Considering the positive charge and lipophilic nature of **[D-2](PF₆)₂** and **[L-2](PF₆)₂**, and the experimental facts highlighted above, it is proposed that upon crossing the plasma membrane, both complexes target the mitochondria.

Due to the lack of uptake selectivity of **[D-2](PF₆)₂** vs **[L-2](PF₆)₂** and proposed localization in the mitochondria, a final imaging experiment with sodium azide (NaN₃) was realized. Sodium azide treatment is known to inhibit all energy-dependent uptake mechanisms. Cells treated with NaN₃ together with **[D-2](PF₆)₂** or **[L-2](PF₆)₂**, did not show significant differences in uptake or localization (Figure S.II.8) compared to cells that were only treated the ruthenium compounds. Altogether, and although the cytotoxicity of both enantiomers does depend on the chirality of the glucose moiety, these results support a glucose transporter-independent, energy-independent^[19] uptake mechanism *in vitro*.

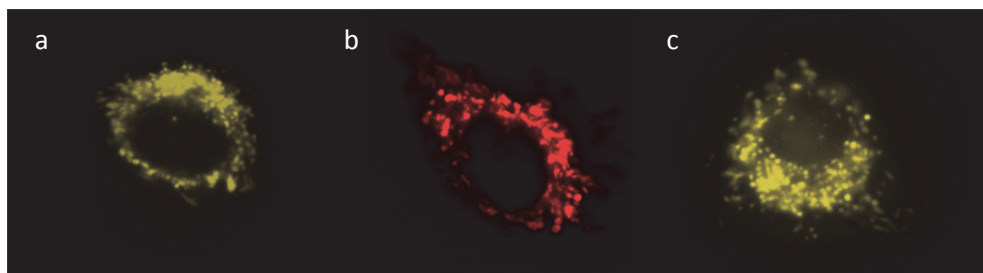


Figure 3.4 Microscopy images of A549 cell treated with (a) **[D-2](PF₆)₂** ($\lambda_{\text{exc}} = 488 \text{ nm}$, $c = 25 \mu\text{M}$), (b) MitoTracker deep red ($\lambda_{\text{exc}} = 639 \text{ nm}$, $c_{\text{final}} = 1.1 \mu\text{M}$), and (c) **[L-2](PF₆)₂** ($\lambda_{\text{exc}} = 488 \text{ nm}$, $c = 25 \mu\text{M}$).

3.2.5 Photochemistry with DNA

The mitochondria house double stranded, circular DNA, which is very interesting given the mitochondrial localization and the DNA light-switch capabilities of dppz analogues of **[D-2](PF₆)₂**.^[20] Therefore, the photochemistry of **[D-2](PF₆)₂** with calf thymus DNA (CT-DNA) and pUC19 plasmid DNA was studied in more detail. As explained above, in PBS under blue light excitation (450 nm) in air the emission maximum of **[D-2](PF₆)₂** shifted from 648 nm to 690 nm, which was attributed to the formation of **[1]²⁺**. In such conditions, there was no significant change in emission intensity over irradiation time (Figure 3.5a). However, under the same irradiation conditions, but in the presence of CT-DNA the emission not only shifted from 648 to 700 nm, but it also increased by 10-fold in intensity over 25 min of irradiation (Figure 3.5b). Under similar conditions, the presence of micelles

(Pluronic F-127), DOPC/DMPC liposomes, L-cysteine, L-histidine, L-glutathione, L-lysine, L-tryptophane and 5'-GMP (5 mM in PBS) did not enhance the emission after irradiation. These data not only confirm a specific DNA light-switch interaction of $[1]^{2+}$ with CT-DNA, but they also provide further support that the emission in cells to be the result of interactions with DNA.

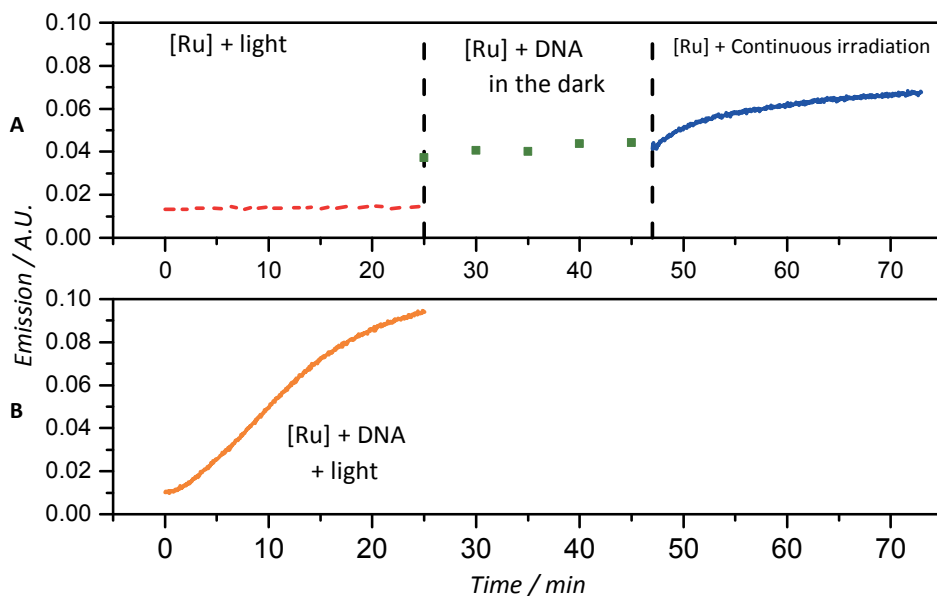


Figure 3.5 a) Emission spectrum of $[D-2](PF_6)_2$ in PBS without DNA (---), with CT-DNA (—) and during continuous irradiation (—). $\lambda_{em} = 707$ nm. b) Emission spectrum of $3.5 \mu\text{M}$ in PBS + CT-DNA during constant blue light irradiation (450 nm).

The emission study suggested different interaction of $[D-2]^{2+}$ and $[1]^{2+}$ with DNA. To further investigate this point interaction of $[D-2](PF_6)_2$ and pUC19 plasmid DNA was further analysed using agarose gel electrophoresis. pUC19 was supplied as a 2686 bp plasmid, of which ~95% was in the supercoiled (SC) form. A single nick in one of the SC strands, caused by 1O_2 for example, results in the open circular (OC) form, which migrates more slowly through the gel than the SC form. Staining and visualization of the DNA using ethidium bromide (EtBr), a known DNA intercalator, is sensitive to the ratio of DNA bp (base pairs) to metal complex (MC, Figure 3.6). Thus, $[D-2]^{2+}$ and EtBr compete for the same DNA binding sites. To determine the photobinding and photocleaving ability of $[D-2]^{2+}$, a 400:1 bp:MC (base pairs:metal complex) ratio was used. At such a low metal complex concentration (~5 μM), $[D-2]^{2+}$ displayed minimal binding in the dark, and also allowed for DNA visualization using EtBr (Figure 3.6). With increasing light doses however ($\lambda_{exc} = 454$ nm, 1 min, $0.6 \text{ J}\cdot\text{cm}^{-2}$, to 15 min, $9.5 \text{ J}\cdot\text{cm}^{-2}$) two phenomena were observed. First, an increased volume of the OC form was observed at increased light doses, which is a sign of 1O_2 generation (Figure S.II.4). Second, migration retardation of the SC form was clearly observed. In our case, a limitation of DNA gel electrophoresis was that the specific mode of interaction (covalent modification vs. intercalation) could not be specified.

However, it did show that photo-induced association of $[1]^{2+}$ or $[D-2]^{2+}$ with the SC form was occurring. Taking into account both sets of DNA experiments, it is proposed that the photoproduct $[1]^{2+}$ is able to interact with mitochondrial DNA either *via* intercalation or *via* coordination, which results in increased emission of the metal complex and DNA photocleavage *via* formation of 1O_2 . Both DNA binding and DNA cleavage occur at very high bp:MC ratio compared to previously reported DNA switches,^[20-21] which highlight the exceptional photodynamic properties of $[1]^{2+}$.

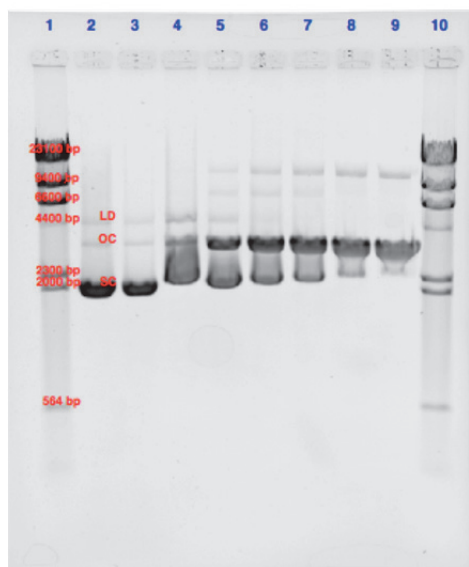


Figure 3.6. Agarose gel showing photoinduced binding and photocleavage of pUC19 plasmid DNA with $[D-2](PF_6)_2$ irradiated for 0-15 min with blue light (455 nm). LD = linear dimer, OC = open circular and SC = supercoiled. Lane 1 = λ MW marker, 2 = DNA control, 37 °C, dark, 3 = DNA control, 37 °C, irradiated, 4 = 400:1 BP:MC, 37 °C, dark, 5 – 9 = 1, 3, 5, 10 and 15 min irradiation, 10 = λ MW marker.

3.3 Conclusions

Glycoconjugation may have two functions in drug design. First, it dramatically improves the hydrophilicity of a compound, which improves drug-likeness for lipophilic compounds such as $[1]^{2+}$. By combining glycoconjugation with the light-induced uncaging properties of ruthenium-based polypyridyl compounds, one can recover the hydrophobic active molecule $[1]^{2+}$ inside the cell providing the glycoconjugated compound can still cross the cell membrane. For $[D-2](PF_6)_2$ and $[L-2](PF_6)_2$ this approach was very successful: the dppn ligand is lipophilic enough to counter-balance the hydrophilicity of the glucose moiety, which allows passive uptake to take place. Upon irradiation with a low dose of visible light (454 nm, $3.2 \text{ J} \cdot \text{cm}^{-2}$) a very high cytotoxic activity characterized by submicromolar EC_{50} values was obtained. The significant phototoxic indices of these compounds may be a

consequence of two photochemical reactions occurring at least in the mitochondria. First, photosubstitution of the thioether-glucose ligand in $[\mathbf{D-2}]^{2+}$ by water occurs, which allows the photoproduct $[\mathbf{1}]^{2+}$ to interact better with biomolecules. In particular, mitochondrial DNA seems a likely target of the achiral photoproduct $[\mathbf{1}]^{2+}$, as it interacts with plasmid DNA at particularly high bp:Ru ratio. Second, both $[\mathbf{2}]^{2+}$ and $[\mathbf{1}]^{2+}$ efficiently generate $^1\text{O}_2$, which for adducts between mitochondrial DNA and $[\mathbf{1}]^{2+}$ leads to extensive DNA photocleavage. To our knowledge, these results represent the first practical demonstration that photosubstitution and singlet oxygen generation can combine *in vitro* into a dual mode-of-action resulting in highly efficient light-induced cancer cell death.

The second function of glycoconjugation is to introduce specific interactions between the (pro)drug and glucose-sensitive enzymes. Increased cytotoxicities measured for D-glucose-appended drugs, for example vs. their aglycon analogues, are often interpreted as a sign of glucose transporter-mediated uptake. A similar interpretation would have led us to conclude that the higher dark cytotoxicity of $[\mathbf{D-2}](\text{PF}_6)_2$ vs. $[\mathbf{L-2}](\text{PF}_6)_2$ was the result of glucose transporters being targeted by the D-glucose functional group in $[\mathbf{D-2}](\text{PF}_6)_2$. However, *in vitro* imaging showed no difference in uptake or cellular localization between the two enantiomers, and addition of sodium azide concluded to energy-independent drug uptake. These results demonstrate that GLUT or SGLT are not involved in the uptake of these compounds, and thus that other enzymes, such as for example efflux pumps and/or glucosidases,^[22] must be responsible for the twice higher cytotoxicity of $[\mathbf{D-2}](\text{PF}_6)_2$ in the dark, compared to $[\mathbf{L-2}](\text{PF}_6)_2$. This work has also unexpected consequences: although $[\mathbf{D-2}](\text{PF}_6)_2$, *i.e.*, the complex conjugated to the natural D-glucose moiety, would be expected to be the most interesting “targeting” enantiomer, $[\mathbf{L-2}](\text{PF}_6)_2$, *i.e.*, the complex conjugated to the non-natural L-glucose moiety, actually shows a higher phototoxic index because of its lower cytotoxicity in the dark. In the end, L-glucose derivatization showed a better pharmacological outcome than functionalization with D-glucose.

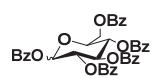
3.4 Experimental

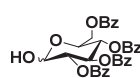
3.4.1 General

Reagents were purchased from Sigma-Aldrich and used without further purification. Benzo[*i*]dipyrido-[3,2-*a*:2',3'-*c*]phenazine (dppn) was synthesized according to a literature procedure.^[23] 2,2':6',2''-Terpyridine (tpy) was ordered from ABCR GmbH & Co. Dry solvents were collected from a Pure Solve MD5 dry solvent dispenser from Demaco. For all inorganic reactions solvents were deoxygenated by bubbling argon through the solution for 30 minutes. Flash chromatography was performed on silica gel (Screening devices B.V.) with a particle size of 40 - 64 μM and a pore size of 60 Å. TLC analysis was conducted on TLC aluminium foils with silica gel matrix (Supelco, silica gel 60, 56524) with detection by UV-absorption (254 nm), by spraying with 10% H_2SO_4 in ethanol or with a solution of

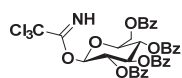
$\text{NH}_4\text{Mo}_7\text{O}_{24} \cdot 4\text{H}_2\text{O}$ 25 g/L, $\text{NH}_4\text{CeSO}_4 \cdot \text{H}_2\text{O}$ 10 g/L, 10% H_2SO_4 in H_2O , followed by charring at $\sim 250^\circ\text{C}$ on a heating plate. Optical rotation measurements were performed on a Propol automated polarimeter (sodium D-line, $\lambda = 589\text{ nm}$) with a concentration of 10 mg/mL ($c = 1$) unless stated otherwise. Infrared spectra were recorded on a Perkin Elmer UATR (Single Reflection Diamond) Spectrum Two device ($4000\text{--}700\text{ cm}^{-1}$; resolution 4 cm^{-1}). ^1H NMR and ^{13}C NMR were recorded in $[\text{D}_6]\text{DMSO}$, CD_3OD and CDCl_3 with chemical shift (δ) relative to the solvent peak. High resolution mass spectra were recorded by direct injection ($2\text{ }\mu\text{L}$ of $2\text{ }\mu\text{M}$ solution in water/acetonitrile; 50/50; v/v and 0.1% formic acid) in a mass spectrometer (Thermo Finnigan LTQ Orbitrap) equipped with an electrospray ion source in positive mode (source voltage 3.5 kV, sheath gas flow 10, capillary temperature 250°C) with resolution $R = 60000$ at m/z 400 (mass range $m/z = 150\text{--}2000$) and dioctylphthalate ($m/z = 391.28428$) as a lock mass. The high-resolution mass spectrometer was calibrated prior to measurements with a calibration mixture (Thermo Finnigan). Elemental analysis was performed at Kolbe Mikrolab Germany.

3.4.2 Synthesis

 **1,2,3,4,6-Penta-O-benzoyl- α/β -L-glucopyranose, L-6:** To a solution of L-glucose^[24] (627 mg, 3.47 mmol) in pyridine (17.0 mL) at 0°C , was slowly added benzoyl chloride (2.20 mL, 18.9 mmol). The suspension was allowed to stir for 6 h at room temperature, after which excess benzoyl chloride was neutralized upon the addition of water (10 mL), resulting in a clear solution. The solution was further diluted with EtOAc ($\sim 100\text{ mL}$) and washed with 1 M HCl (2x), NaHCO_3 (aq). (2x) and brine (2x). Layers were separated, and the organic layer was dried over Na_2SO_4 and subsequently concentrated *in vacuo*. Purification over silica (0 to 10% MeOH in DCM) afforded the title compound as a white solid (2.43 g, 3.47 mmol, quant. α/β ratio of 1:2). The analytical data are in agreement with those reported in literature^[25], but the sign of the specific rotation was found opposite. $[\alpha]_{\text{D}}^{20} (\text{CHCl}_3)$: +49.2 (α/β 1:2).

 **2,3,4,6-Tetra-O-benzoyl- α,β -L-glucopyranose, L-7:** To a cooled solution of L-6 (3.01 g, 4.30 mmol) in DCM (10 mL) was added 33% HBr in AcOH (2.50 mL, 10.2 mmol). The resulting yellow/orange solution was allowed to stir overnight, after which it was diluted with EtOAc (250 mL) followed by washing NaHCO_3 aq. (2x), H_2O (2x) and brine (2x). Layers were separated and the organic layer was dried over Na_2SO_4 and concentrated *in vacuo*. The crude was dissolved in acetone (15 mL) and water (0.40 mL) and Ag_2CO_3 (650 mg, 2.36 mmol) were added. The suspension was allowed to stir at room temperature for 3 h, after it was filtrated over Celite® and concentrated *in vacuo*, affording the title compound as a white foam (2.43 g, 4.26 mmol, 99%, α/β ratio of

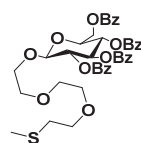
1:1). The analytical data are in agreement with those reported in literature^[26], but the sign of the specific rotation was found opposite. α -anomer: $[\alpha]_{\text{D}}^{20} (\text{CHCl}_3)$: -68.2°



2,3,4,6-Tetra-O-benzoyl-1- β -L-glucopyranosyl trichloroacetimidate, L-8:

To a solution of L-7 (2.19 g, 3.67 mmol) and in dry DCM was added DBU (0.60 mL, 4.02 mmol) and trichloroacetonitrile (13.0 mL, 130 mmol).

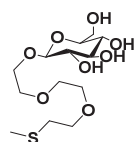
This solution was allowed to stir overnight, after which it was concentrated *in vacuo*. Purification of the crude over silica (33% EtOAc in PE) afforded the title compound as an off-white foam (2.12 g, 2.86 mmol, 78%, α/β ratio of 1:1). The analytical data are in agreement with those reported in literature,^[27] but the sign of the specific rotation was found opposite. α -anomer: $[\alpha]_{\text{D}}^{20} (\text{CHCl}_3)$: -62.0°



2-[2-(2-(Methylthio)ethoxy)ethoxy]ethyl 2,3,4,6-tetra-O-benzoyl- β -L-glucopyranoside, L-9:

This compound was prepared as described for 2-[2-(2-(Methylthio)ethoxy)ethoxy]ethyl 2,3,4,6-tetra-O-benzoyl- β -D-glucopyranoside (Chapter 2), but starting from L-8 (2.12 g, 2.86 mmol).

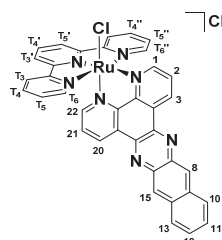
Yield: 1.49 g, 1.96 mmol, 69%. L-9 has the same spectroscopic properties as its enantiomer, however with the opposite sign of rotation. $[\alpha]_{\text{D}}^{20} (\text{CHCl}_3)$: -18.0 .



2-[2-(2-(Methylthio)ethoxy)ethoxy]ethyl β -L-glucopyranoside, L-3:

This compound was prepared as described for (2-Methylthio)ethyl- β -D-glucopyranoside (Chapter 2) but starting from L-9 (1.47 g, 1.99 mmol) Yield:

580 mg, 1.69 mmol, 85%. L-3 has the same spectroscopic properties as its enantiomer, however with opposite sign of rotation. $[\alpha]_{\text{D}}^{20} (\text{MeOH})$: $+11.8$.

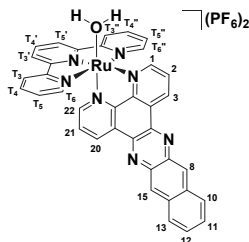


[Ru(tpy)(dppn)Cl]Cl, [4]Cl:

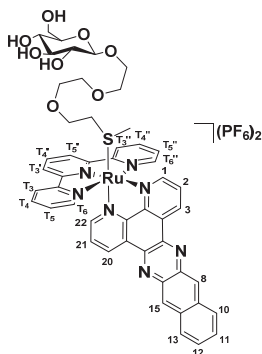
Ruthenium dimer $[\{\text{Ru}(\text{tpy})\text{Cl}_2\}_2] \cdot \text{H}_2\text{O}$ ^[28] (300 mg, 0.347 mmol) and dppn^[23] (231 mg, 0.695 mmol) were dissolved in a deoxygenated solution of ethylene glycol (17 mL) which was heated to 100 °C under an argon atmosphere for five h. The resulting purple solution was then filtered over Celite®. Addition of Et₂O to the filtrate resulted in a precipitate which was collected on a glass frit and thoroughly washed with water and

Et₂O, followed by drying under high vacuum which furnished the title compound as a purple powder (383 mg, 0.473 mmol, 75%). R_f = 0.31 (10% MeOH in DCM). ¹H NMR (400 MHz, [D₆]DMSO) δ = 10.42 (d, J = 4.7 Hz, 1H, 1), 9.75 (d, J = 8.0 Hz, 1H, 3), 9.21 – 9.06 (m, 3H, 8, 22, 15), 8.90 (d, J = 8.1 Hz, 2H, T₃', T₅'), 8.75 (d, J = 8.1 Hz, 2H, T₆', T₆''), 8.56 (dd, J = 8.1, 5.4 Hz, 1H, 2), 8.38 (d, J = 9.5 Hz, 1H, T₃, T₃''), 8.30 (t, J = 8.1 Hz, 1H, T₄'), 7.99 (t, J = 8.1 Hz, 2H, T₅, T₅''), 7.83 (d, J = 5.4 Hz, 1H, 20), 7.78 – 7.65 (m, 4H, 10, 13, T₄, T₄''), 7.53 (dd, J = 8.1, 5.5 Hz, 1H, 21), 7.32 (t, J = 6.7 Hz, 2H, 11, 12); ¹³C NMR (100 MHz, DMSO) δ = 158.4

(C_q), 157.6 (C_q), 154.0 (C_H 1), 153.80 (C_H 20), 152.6 (C_q), 152.5 (C_H 10, C_H 13), 150.5 (C_q), 141.5 (C_q), 141.0 (C_q), 137.9 (C_q), 137.8 (C_q), 137.2 (C_H T₅, C_H T₅''), 134.5 (C_q), 134.4 (C_q), 134.2 (C_H T₄'), 131.9 (C_H 3), 130.8 (C_H 8), 130.1 (C_q), 129.6 (C_q), 128.5 (C_H T₃), 128.5 (C_H T₃''), 127.9 (C_H 22), 127.8 (C_H 15), 127.3 (C_H T₄, T₄''), 127.2 (C_H 11, C_H 12), 126.5 (C_H 21), 123.7 (C_H 21), 122.80 (C_H T₃', C_H T₅'); HRMS *m/z* calcd for [C₃₇H₂₃N₇ClRu – Cl]: 702.07415; found: 702.07439. Elemental analysis calcd (%) for C₃₇H₂₃N₇Ru.4H₂O: C 54.89, H 3.86, N 12.11; found: C 53.63, H 3.83, N 11.61.



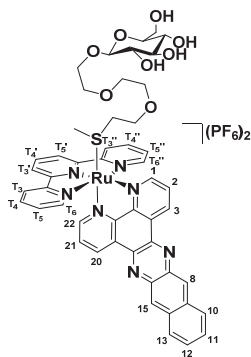
[Ru(tpy)(dppn)(H₂O)](PF₆)₂, [1](PF₆)₂: To a solution of **[4]Cl** (73.0 mg, 0.099 mmol) in acetone/water (10 mL, 3:1) was added AgNO₃ (39.0 mg, 0.230 mmol). This mixture was allowed to stir under argon at 50 °C for 16 h, after which it was filtered over Celite®. 2 mL of a saturated solution of NH₄PF₆ was added to the filtrate and the resulting brown precipitate was collected on a glass frit, followed by washing with H₂O (3x) and Et₂O (3x), affording **[10](PF₆)₂** as a brown precipitate (60 mg, 0.083 mmol, 84%) which was used without further purification. *R_f* = 0.5 (100/80/20 acetone/water/sat. aq. KPF₆).



[Ru(tpy)(dppn)(D-3)](PF₆)₂, [D-2](PF₆)₂: **[1](PF₆)₂** (60.0 mg, 0.0668 mmol) and ligand **D-3** (61.0 mg, 0.178 mmol) were dissolved in deoxygenated acetone and stirred at 50 °C for 24 h under an argon atmosphere in the dark. The resulting brown/orange solution was concentrated *in vacuo* at 30 °C in the dark, followed by purification of the crude over silica (acetone/water/saturated aqueous KPF₆ 100:0:0 to 80:20:0 to 100:80:20) followed by further purification over Sephadex LH-20 (acetone). The orange fraction was collected and the volume was reduced to ~10%, followed by addition of Et₂O, resulting in

a precipitate which was collected by filtration over a Whatman® RC60 membrane filter and subsequently washed with EtOAc (3x), Et₂O (3x) and *n*-hexane (3x), affording the title compound as an orange powder (30 mg, 23 μmol, 35%). *R_f* = 0.36 (16:4:1 acetone/water/sat. KPF₆); ¹H NMR (400 MHz, [D₆]acetone) δ = 10.39 (d, *J* = 5.4 Hz, 1H, 1), 10.09 (d, *J* = 8.2 Hz, 1H, 3), 9.60 (d, *J* = 8.3 Hz, 1H, 22), 9.27 (s, 1H, 8), 9.15 (s, 1H, 15), 9.03 (d, *J* = 8.2 Hz, 2H, T₃', T₅'), 8.84 (d, *J* = 8.0 Hz, 2H, T₆, T₆''), 8.73 (dd, *J* = 8.3, 5.3 Hz, 1H, 2), 8.61 (t, *J* = 8.2 Hz, 1H, T₄'), 8.44 (dd, *J* = 18.7, 9.0 Hz, 2H, 11, 12), 8.19 (t, *J* = 7.9 Hz, 2H, T₅, T₅''), 8.13 (t, *J* = 3.7 Hz, 2H, T₄, T₄''), 8.06 (d, *J* = 5.4 Hz, 1H, 20), 7.84 – 7.76 (m, 3H, 21, 10, 13), 7.47 (t, *J* = 6.6 Hz, 2H, T₃, T₃''), 4.31 (d, *J* = 7.7 Hz, 1H, H-1), 4.23 (dd, *J* = 12.9, 3.5 Hz, 1H, CHH H-6), 3.99 – 3.92 (m, 1H, CHH OCH₂), 3.86 – 3.76 (m, 1H, CHH OCH₂), 3.71 – 3.51 (m, 12H, CHH H-6, 2 x CHH OCH₂, 3 x CH₂ OCH₂), 3.41 – 3.23 (m, 3H, H-3, H-4, H-5), 3.11 (td, *J* = 8.2, 3.5 Hz, 1H, H-2), 2.26 – 2.18 (m, 2H, CH₂ OCH₂SMe), 1.66 (s, 3H). ¹³C NMR (100

MHz, [D₆]acetone) δ = 159.0 (C_q), 158.5 (C_q), 155.0 (C_H 1), 153.2 (C_H 1, C_H T₃, C_H T₃''), 139.4 (C_H T₅, C_H T₅''), 138.3 (C_H T₄'), 136.0 (C_q), 135.0 (C_H 3) 134.7 (C_H 22), 132.5 (C_q), 131.4 (C_q), 129.5 (C_H T₄, C_H T₄''), 129.5 (C_H 11, C_H 12) 129.1 (C_H 8, C_H 15), 128.9 (C_H 11, C_H 5, C_H 8), 128.0 (H_{arom}), 126.1 (C_H T₆, C_H T₆''), 125.4 (C_H T₃', C_H T₅'), 104.2 (C-1), 78.0 (C-3), 77.5 (C-4), 74.8 (C-2), 71.7 (C-5), 71.0 (2 x CH₂ OCH₂), 70.9 (CH₂ OCH₂), 69.3 (CH₂ OCH₂), 68.2 (CH₂ OCH₂), 62.9 (C-6), 35.6 (CH₂ OCH₂SMe), 15.6 (OCH₂SMe); HRMS m/z calcd for [C₅₀H₄₉O₈N₇SRu – 2PF₆]: 504.61979; found: 504.61993. Elemental analysis calcd (%) for [D-2](PF₆)₂: C 46.23, H 3.80, N 7.55; found: C 46.26, H 3.81, N 7.53.



[Ru(tpy)(dppn)(L-3)](PF₆)₂, [L-2](PF₆)₂: This compound was synthesized and purified according to the procedure described for compound [D-2](PF₆)₂, starting from ligand L-3 (94.0 mg, 0.0964 mmol) instead of D-3. This procedure afforded [L-2](PF₆)₂ as an orange powder (40 mg, 0.031 mmol, 32%). ¹H NMR and HRMS matched those reported for [D-2](PF₆)₂. Elemental analysis for [L-2](PF₆)₂·H₂O: C 45.60, H 3.90, N 7.44; found: C 45.70, H 4.06, N 7.32.

3.4.3 Emission spectroscopy: Interaction with DNA

0.15 mL of a stock solution of [D-2](PF₆)₂ (14 μM) was prepared in phosphate buffer and was diluted with PBS (0.30 mL) in a semi-micro cuvette (4.7 μM), followed by 450 nm irradiation of the sample for 25 minutes (50 mW, 4 mm beam diameter, 8% of the sample simultaneously irradiated). During this period, emission spectra were continuously recorded. At the end of irradiation, [D-2](PF₆)₂ had been fully converted to the aqua complex [1](PF₆)₂. Then, 0.15 mL of a solution of sonicated calf thymus DNA was added to reach a final DNA concentration of 0.5 mg/mL, leading to a strong increase of the emission. The sample was left in the dark, while emission spectra were recorded at an interval of five minutes until $t = 45$ minutes; no major variation of the emission intensity was observed. After this period, the sample was irradiated continuously again, which led to a gradual increase of the emission intensity. In a parallel experiment, CT-DNA and [D-2](PF₆)₂ were mixed directly at $t = 0$ and the sample was irradiated at 450 nm for 25 min while recording emission spectra continuously. In such conditions the emission intensity increased in a sigmoidal curve, suggesting cleavage of the thioether-glucose conjugate and switched on emission following insertion of the dppn ligand between DNA based pairs.

3.4.4 Photochemistry

3.4.4.5 General procedure for photosubstitution quantum yield measurements

3.00 mL of a solution of [D-2](PF₆)₂ (4.23×10⁻⁵ M) in H₂O was deoxygenated for 15 minutes with dinitrogen gas, after which it was irradiated with a blue LED (447 nm, FWHM: 19 nm) with photon flux $\Phi = 1.77 \cdot 10^{-7}$ mol photons · s⁻¹ while the solution was kept at constant temperature (25 °C). During irradiation UV-vis spectra were recorded on a Varian Inc. Cary 50 UV-vis spectrometer with intervals of 30 seconds until t = 3600 seconds. ESI-MS spectra were recorded after the irradiation experiment to confirm the formation of the aqua species [Ru(tpy)(dppn)(OH₂)]²⁺ (m/z = found 342.4, calculated 342.5). The quantum yield for the photosubstitution of the thioether ligand was calculated according to the method described earlier.^[29] Reference molar absorption coefficients used to calculate concentrations during irradiation are provided in Table 3.3.

Table 3.3 Reference wavelengths (λ_{ref}) and molar absorption coefficients (ϵ_{ref}) for photosubstitution quantum yield calculations.

Compound	λ_{ref} in nm	ϵ_{ref} (M ⁻¹ cm ⁻¹)
[1](PF ₆) ₂	490	10.8 × 10 ³
	430	12.4 × 10 ³
[D-2](PF ₆) ₂	490	10.5 × 10 ³
	430	7.4 × 10 ³

3.4.4.6 ¹O₂ and phosphorescence quantum yield measurements

See general appendix I.1.1 and Figure S.II.2.

3.4.5 Biology

Cytotoxicity studies were carried out as described in appendix 1.2.1. A detailed description of the DNA interaction studies and emission microscopy experiments are given in appendix II.2.

References

- [1] a). D. Deng, C. Xu, P. Sun, J. Wu, C. Yan, M. Hu, N. Yan, *Nature* **2014**, *510*, 121-125; b). K. O. Alfarouk, D. Verduzco, C. Rauch, A. K. Muddathir, H. H. B. Adil, G. O. Elhassan, M. E. Ibrahim, J. David Polo Orozco, R. A. Cardone, S. J. Reshkin, S. Harguindey, *Oncoscience* **2014**, *1*, 777-802.
- [2] a). M. M. Welling, R. Alberto, *Nucl Med Commun* **2010**, *31*, 239-248; b). C. L. Ferreira, S. R. Bayly, D. E. Green, T. Storr, C. A. Barta, J. Steele, M. J. Adam, C. Orvig, *Bioconjugate Chem* **2006**, *17*, 1321-1329.
- [3] E. C. Calvaresi, P. J. Hergenrother, *Chem Sci* **2013**, *4*, 2319-2333.
- [4] a). E. C. Calvaresi, C. Granchi, T. Tuccinardi, V. Di Bussolo, R. W. Huigens, 3rd, H. Y. Lee, R. Palchaudhuri, M. Macchia, A. Martinelli, F. Minutolo, P. J. Hergenrother, *ChemBiochem* **2013**, *14*, 2263-2267; b). D. N. Pelageev, S. A. Dyshlovoy, N. D.

- Pokhilo, V. A. Denisenko, K. L. Borisova, G. Keller-von Amsberg, C. Bokemeyer, S. N. Fedorov, F. Honecker, V. P. Anufriev, *Eur J Med Chem* **2014**, *77*, 139-144.
- [5] a). U. Basu, I. Khan, A. Hussain, B. Gole, P. Kondaiah, A. R. Chakravarty, *Inorg Chem* **2014**, *53*, 2152-2162; b). W. H. Law, L. C. Lee, M. W. Louie, H. W. Liu, T. W. Ang, K. K. Lo, *Inorg Chem* **2013**, *52*, 13029-13041; c). P. Liu, Y. Lu, X. Gao, R. Liu, D. Zhang-Negrierie, Y. Shi, Y. Wang, S. Wang, Q. Gao, *Chem Commun* **2013**, *49*, 2421-2423; d). R. Schibli, C. Dumas, J. Petrig, L. Spadola, L. Scapozza, E. Garcia-Garayoa, P. A. Schubiger, *Bioconjugate Chem* **2005**, *16*, 105-112; e). M. L. Bowen, C. Orvig, *Chem Commun* **2008**, 5077-5091.
- [6] B. Banik, K. Somyajit, A. Hussain, G. Nagaraju, A. R. Chakravarty, *Dalton Trans* **2014**, *43*, 1321-1331.
- [7] J. Park, J. I. Um, A. Jo, J. Lee, D. W. Jung, D. R. Williams, S. B. Park, *Chem Commun* **2014**, *50*, 9251-9254.
- [8] M. Patra, T. C. Johnstone, K. Suntharalingam, S. J. Lippard, *Angew Chem Int Ed* **2016**, *55*, 2550-2554.
- [9] C. Barron, E. Tsiani, T. Tsakiridis, *BMC Proc* **2012**, *6*, P4.
- [10] J. Pohl, B. Bertram, P. Hilgard, M. R. Nowrousian, J. Stuben, M. Wiessler, *Cancer Chemother Pharmacol* **1995**, *35*, 364-370.
- [11] a). Y. Liu, Y. Cao, W. Zhang, S. Bergmeier, Y. Qian, H. Akbar, R. Colvin, J. Ding, L. Tong, S. Wu, J. Hines, X. Chen, *Mol Cancer Ther* **2012**, *11*, 1672-1682; b). W. K. Miskimins, H. J. Ahn, J. Y. Kim, S. Ryu, Y. S. Jung, J. Y. Choi, *PLoS One* **2014**, *9*, e85576; c). A. Dilip, G. Cheng, J. Joseph, S. Kunnimalaiyaan, B. Kalyanaraman, M. Kunnimalaiyaan, T. C. Gamblin, *Anticancer Drugs* **2013**, *24*, 881-888.
- [12] L. Venturelli, S. Nappini, M. Bulfoni, G. Gianfranceschi, S. Dal Zilio, G. Coceano, F. Del Ben, M. Turetta, G. Scoles, L. Vaccari, D. Cesselli, D. Cojoc, *Sci Rep* **2016**, *6*, 21629.
- [13] D. Deng, P. Sun, C. Yan, M. Ke, X. Jiang, L. Xiong, W. Ren, K. Hirata, M. Yamamoto, S. Fan, N. Yan, *Nature* **2015**, *526*, 391-396.
- [14] a). R. E. Goldbach, I. Rodriguez-Garcia, J. H. van Lenthe, M. A. Siegler, S. Bonnet, *Chem Eur J* **2011**, *17*, 9924-9929; b). B. S. Howerton, D. K. Heidary, E. C. Glazer, *J Am Chem Soc* **2012**, *134*, 8324-8327; c). T. Respondek, R. N. Garner, M. K. Herroon, I. Podgorski, C. Turro, J. J. Kodanko, *J Am Chem Soc* **2011**, *133*, 17164-17167; d). V. H. S. van Rixel, B. Siewert, S. L. Hopkins, S. H. C. Askes, A. Busemann, M. A. Siegler, S. Bonnet, *Chem Sci* **2016**, *7*, 4922-4929; e). M. A. Sgambellone, A. David, R. N. Garner, K. R. Dunbar, C. Turro, *J Am Chem Soc* **2013**, *135*, 11274-11282; f). L. Zayat, C. Calero, P. Albores, L. Baraldo, R. Etchenique, *J Am Chem Soc* **2003**, *125*, 882-883.
- [15] a). D. Crespy, K. Landfester, U. S. Schubert, A. Schiller, *Chem Commun* **2010**, *46*, 6651-6662; b). U. Schatzschneider, *Eur J Inorg Chem* **2010**, *2010*, 1451-1467; c). C. Mari, V. Pierroz, S. Ferrari, G. Gasser, *Chem Sci* **2015**, *6*, 2660-2686; d). N. J. Farrer, L. Salassa, P. J. Sadler, *Dalton Trans* **2009**, 10690-10701; e). A. Presa, R. F. Brissos, A. B. Caballero, I. Borilovic, L. Korrodi-Gregorio, R. Perez-Tomas, O. Roubeau, P. Gamez, *Angew Chem Int Ed* **2015**, *54*, 4561-4565.
- [16] X. Zhu, R. R. Schmidt, *Angew Chem Int Ed* **2009**, *48*, 1900-1934.

- [17] J. D. Knoll, B. A. Albani, C. Turro, *Chem Commun* **2015**, 51, 8777-8780.
- [18] H. Huang, B. Yu, P. Zhang, J. Huang, Y. Chen, G. Gasser, L. Ji, H. Chao, *Angew Chem Int Ed* **2015**, 54, 14049-14052.
- [19] A. C. Komor, J. K. Barton, *Chem Commun* **2013**, 49, 3617-3630.
- [20] a). A. E. Friedman, J.-C. Chambron, J.-P. Sauvage, N. J. Turro, J. K. Barton, *J Am Chem Soc* **1990**, 112, 4960-4962; b). H. Niyazi, J. P. Hall, K. O'Sullivan, G. Winter, T. Sorensen, J. M. Kelly, C. J. Cardin, *Nat Chem* **2012**, 4, 621-628.
- [21] a). H. Song, J. T. Kaiser, J. K. Barton, *Nat Chem* **2012**, 4, 615-620; b). Y. Sun, L. E. Joyce, N. M. Dickson, C. Turro, *Chem Commun* **2010**, 46, 2426-2428.
- [22] H. Seker, B. Bertram, A. Burkle, B. Kaina, J. Pohl, H. Koepsell, M. Wiesser, *Br J Cancer* **2000**, 82, 629-634.
- [23] A. J. McConnell, M. H. Lim, E. D. Olmon, H. Song, E. E. Dervan, J. K. Barton, *Inorg Chem* **2012**, 51, 12511-12520.
- [24] R. F. Martinez, Z. Liu, A. F. Glawar, A. Yoshihara, K. Izumori, G. W. Fleet, S. F. Jenkinson, *Angew Chem Int Ed* **2014**, 53, 1160-1162.
- [25] D. Sail, P. Kovac, *Carbohydr Res* **2012**, 357, 47-52.
- [26] A. E. Salinas, J. F. Sproviero, V. Deulofeu, *Carbohydr Res* **1987**, 170, 71-99.
- [27] I. A. Ivanova, A. J. Ross, M. A. J. Ferguson, A. V. Nikolaev, *J Chem Soc Dalton* **1999**, 1743-1754.
- [28] D. C. Marelus, S. Bhagan, D. J. Charboneau, K. M. Schroeder, J. M. Kamdar, A. R. McGettigan, B. J. Freeman, C. E. Moore, A. L. Rheingold, A. L. Cooksy, D. K. Smith, J. J. Paul, E. T. Papish, D. B. Grotjahn, *Eur J Inorg Chem* **2014**, 676-689.
- [29] A. Bahreman, J. A. Cuello-Garibo, S. Bonnet, *Dalton Trans* **2014**, 43, 4494-4505.